

Supplementary Information

Doping Molecular Organic Semiconductors by Diffusion from the Vapor Phase

Kelly A. Peterson,¹ Ashlea Patterson,¹ Alejandro Vega-Flick,² Bolin Liao,² Michael L. Chabinyc¹

¹Materials Department, University of California, Santa Barbara, California 93106, United States

² Department of Mechanical Engineering, University of California, Santa Barbara, California 93106, United States

Corresponding Author

* E-mail: mchabinyc@engineering.ucsb.edu

Experimental Methods

Sample Preparation

All materials were used as received. Spiro-OMeTAD (Lumtec) films were spun cast on cleaned quartz substrates from 170 mg/mL solution in chlorobenzene (Sigma Aldrich, anhydrous, 99.8%) at 2000 rpm/s for 45 s under N₂ atmosphere. Gold contacts (80 nm) were evaporated on films for conductivity or Seebeck measurements through a shadow mask. Substrates were attached with tape to the lid of a glass doping chamber with F₄TCNQ (TCI America) in the bottom. The doping chamber was heated on a hot plate at 200 °C in N₂ atmosphere to diffuse F₄TCNQ vapor into the films. Films were annealed at 150 °C for 10 min. To measure the undoped spiro-OMeTAD thermal diffusivity, a pink-dyed film was prepared by blade-coating a chlorobenzene solution containing 1.4 mg/mL Oil Red O (Sigma Aldrich) and 162 mg/mL spiro-OMeTAD on a quartz substrate at 60 °C for an intended 5 mol% Oil Red O film.

Physical Characterization

Film thicknesses were measured on a Bruker DektakXT stylus profilometer. SIMS was performed on a Cameca IMS 7f Auto SIMS with oxygen ion source. GIWAXS was performed at beamline

11-3 at the Stanford Synchrotron Radiation Lightsource, SLAC National Accelerator Laboratory. GIWAXS samples were prepared on native oxide silicon substrates. X-ray incident angle was 0.1° , sample-detector distance was 315 mm, and exposure time was 350-400 s. GIWAXS data was processed using IgorPro packages Nika¹ and WAXStools.²

Spectroscopic Characterization

UV-Vis-NIR film spectra were collected on a Shimadzu UV3600 or PerkinElmer Lambda 750 spectrometer.

Charge Transport Measurements

Room-temperature conductivity was measured under N_2 atmosphere using the four-point probe method with a Keithley 6220 precision current source and Keithley 2400. Low-temperature conductivity was measured under vacuum in a liquid nitrogen-cooled LakeShore Cryotronics TTP probe station. Low-temperature conductivity was measured using the transmission line method with a Keithley 6487 picoammeter. In-plane Seebeck coefficient was measured at room temperature under N_2 atmosphere with a custom probe station. The sample was placed across two Peltier elements that were alternately cooled to create a temperature gradient across the film. The temperature gradient was measured by type T thermocouples on the sample surface with a Fluke 1529 Chub E-4, and the potential gradient was measured with a Keithley 2400.

Thermal Diffusivity

Thermal diffusivity was measured with the transient grating technique on spiro-OMeTAD films on quartz substrates. Extensive details of the transient grating technique can be found in Reference ³. Briefly, a pulsed laser beam at 515 nm from a Yb-doped fiber laser (Clark-MRX IMPULSE) is split by a phase mask and recombined by a confocal imaging system onto the sample surface to form a one-dimensional optical intensity grating. This intensity grating is absorbed by the spiro-OMeTAD film, creating a temperature change with a sinusoidal spatial profile, or a "temperature grating." The decay of the amplitude of this "temperature grating" in time is monitored by the diffraction of a continuous-wave laser (532 nm), which is detected by a fast photodiode (Hamamatsu C5658) and an oscilloscope (Tektronix TDS 784A). This real-time decay

signal is analyzed using a thermal transport model, from which the thermal diffusivity of the spiro-OMeTAD films can be extracted.

Heat capacity was measured on a powder sample of spiro-OMeTAD with a TA Instruments Q2000 differential scanning calorimeter. The sample was subjected to three melting-cooling cycles before measuring the reversing heat capacity during a modulated heating from 15 to 35 °C with a modulation of ± 1 °C every 100 s.

Computational Methods

Geometry of spiro-OMeTAD was optimized at the 6-31G(d)/ ω B97-XD level without symmetry constraints using the default value of ω (0.2 Bohr⁻¹) in Gaussian 16.⁴

Vapor Doping

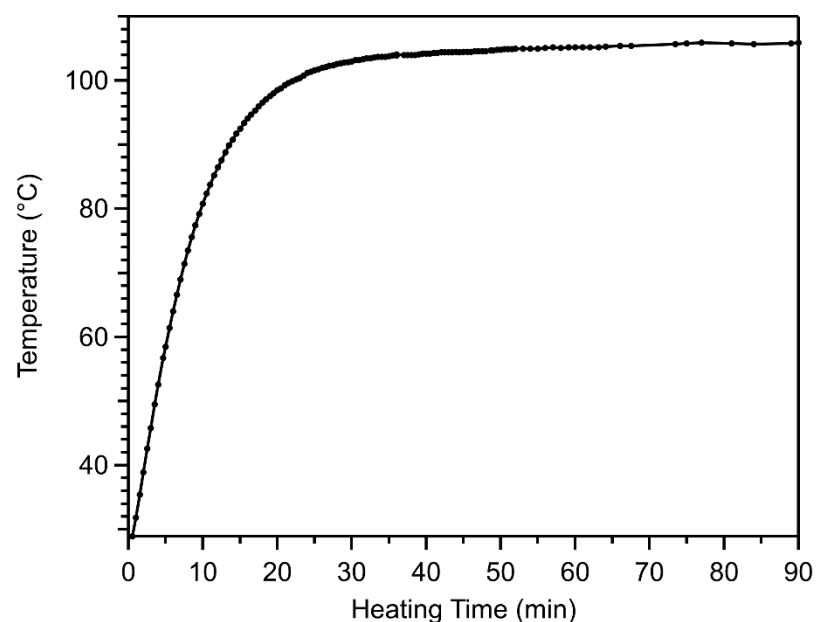


Figure S 1. Temperature of substrate in vapor doping chamber vs. time heated at 200 °C. Temperature is nearly level after 30 min, only increasing from 103-106 °C during the last 60 min of heating.

GIWAXS Linecuts

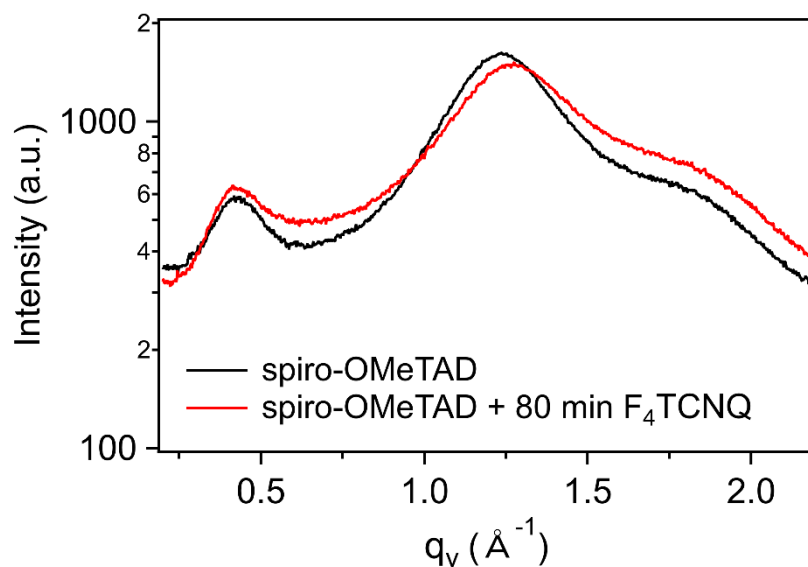


Figure S 2. Q_y linecuts of undoped (black) and 80 min F_4TCNQ vapor doped (red) spiro-OMeTAD from GIWAXS scattering.

F_4TCNQ Anion Reference

We synthesized $[Cp^*_2Co][F_4TCNQ]$ and $[Cp^*_2Fe][F_4TCNQ]$ similar to previously reported procedure.⁵ We measured varying concentrations of $[Cp^*_2Co][F_4TCNQ]$ or $[Cp^*_2Fe][F_4TCNQ]$ in acetonitrile in 1 cm quartz cuvettes (Figure S3). Calculating the maximum NIR molar attenuation coefficient, ϵ , from each spectrum resulted in inconsistent ϵ values (Table S1). Fitting the absorbance at the tallest NIR peak for F_4TCNQ^- (857 nm) vs. concentration with a line gives an $\epsilon \sim 35,500 \text{ M}^{-1} \text{ cm}^{-1}$ (Figure S4). This value is lower than the previously measured ϵ value for $[Cp^*_2Co][F_4TCNQ]$ of $\sim 50,000 \text{ M}^{-1} \text{ cm}^{-1}$,⁵ but it is closer to ϵ values $\sim 40,000\text{-}42,000 \text{ M}^{-1} \text{ cm}^{-1}$ reported for other F_4TCNQ anionic compounds (Table S2).^{6,7} Our ϵ value may differ from these previous measurements due to small errors in the ionic compound synthesis or in preparing the reference solutions. We used the average of the fitted NIR F_4TCNQ^- molar attenuation peak areas ($8331 \text{ ev M}^{-1} \text{ cm}^{-1}$) as the reference value for estimating film carrier concentrations. The standard deviation of this average is 12.5%, but to account for any additional sources of error, we estimated the error in the carrier concentrations at 20%.

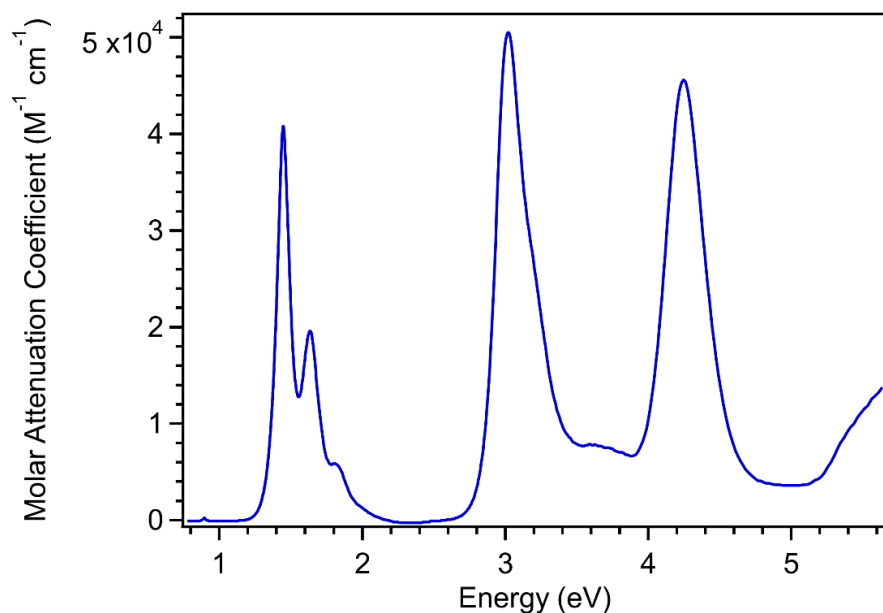


Figure S 3. UV-Vis-NIR molar attenuation coefficient spectrum of $[\text{Cp}^*_2\text{Co}][\text{F}_4\text{TCNQ}]$ 0.0074 mg/mL (12 mM) in acetonitrile in 1 cm quartz cuvette.

Table S 1. F_4TCNQ anion molar attenuation coefficient results from several solution UV-Vis-NIR trials.

Compound	Concentration (mM)	ϵ at 857 nm ($\text{M}^{-1} \text{cm}^{-1}$)	Fitted ϵ NIR area sum ($\text{eV M}^{-1} \text{cm}^{-1}$)
$[\text{Cp}^*_2\text{Co}][\text{F}_4\text{TCNQ}]$	4.1	35,300	7768
$[\text{Cp}^*_2\text{Co}][\text{F}_4\text{TCNQ}]$	8.2	44,200	10,051
$[\text{Cp}^*_2\text{Co}][\text{F}_4\text{TCNQ}]$	8.3	33,300	7325
$[\text{Cp}^*_2\text{Co}][\text{F}_4\text{TCNQ}]$	12	40,900	9016
$[\text{Cp}^*_2\text{Fe}][\text{F}_4\text{TCNQ}]$	17	34,900	7497
Average:		$37,700 \pm 4100$	8331 ± 1044

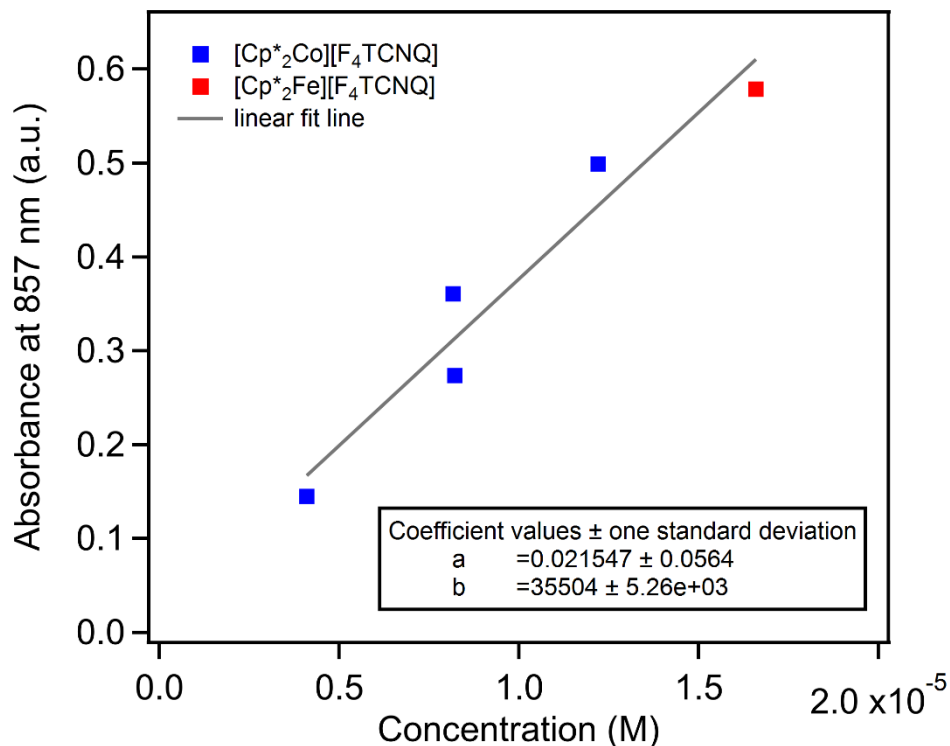


Figure S 4. Plot of NIR absorbance at 857 nm of varying concentrations of [Cp*₂Co][F₄TCNQ] (blue) or [Cp*₂Fe][F₄TCNQ] (red) solution in acetonitrile solution. Slope of linear fit line (b) used to calculate the molar attenuation coefficient, ϵ , of F₄TCNQ⁻ at 857 nm.

Table S 2. Previously reported NIR molar attenuation coefficient (ϵ) values for F₄TCNQ anions.

Compound	Peak ϵ in NIR ($M^{-1} cm^{-1}$)	Ref.
[Cp* ₂ Co][F ₄ TCNQ]	~50,000	⁵
F ₄ TCNQ and excess tetrabutylammonium iodide	~40,000	⁶ (SI)
Li ⁺ F ₄ TCNQ ⁻	~42,000	⁷ (SI)

F₄TCNQ Anion Fitting Method

The area of the three NIR F₄TCNQ anion peaks was used to estimate the carrier concentration of the doped spiro-OMeTAD films for electrical, thermoelectric, and thermal transport measurements. The area of the three peaks was calculated by fitting them using the Multi-peak Fitting package in Igor. The fitting was performed on the section of the spectrum 1.25 – 2.15 eV using a set linear baseline to reduce background effects. For solution spectra, three Voigt peaks (convolution of Gaussian and Lorentzian peaks) were used, with the constraint that they must have the same width and shape factor within the spectrum (Figure S5). The height of peak 1 was constrained as half of the height of peak 0, and the height of peak 2 was constrained as one-fourth the height of peak 1. For the chosen reference spectrum (Figure S5),

the shape factor was 0.56, indicating both Gaussian and Lorentzian contributions to the peak shape.

For film spectra, the same fitting method was used with the addition of a fourth peak for the smaller spiro-OMeTAD⁺ absorbance at 700 nm (1.77 eV) that is obscured by the F₄TCNQ⁻ absorbances. Because this peak has an asymmetric shape, especially at low spiro-OMeTAD⁺ concentrations,⁸ we used the “ExpModGauss” peak shape (convolution of Gaussian peak and exponential decay) to fit this obscured absorbance peak (Figure S6). The location of this peak was constrained between 1.5-1.8 eV and was usually fit to a location 1.7-1.8 eV. For the F₄TCNQ⁻ peak fittings, the Voigt shape parameter was close to zero, indicating a Gaussian peak shape. See Figure S7 for how the calculated carrier concentration estimates correspond to vapor doping time.

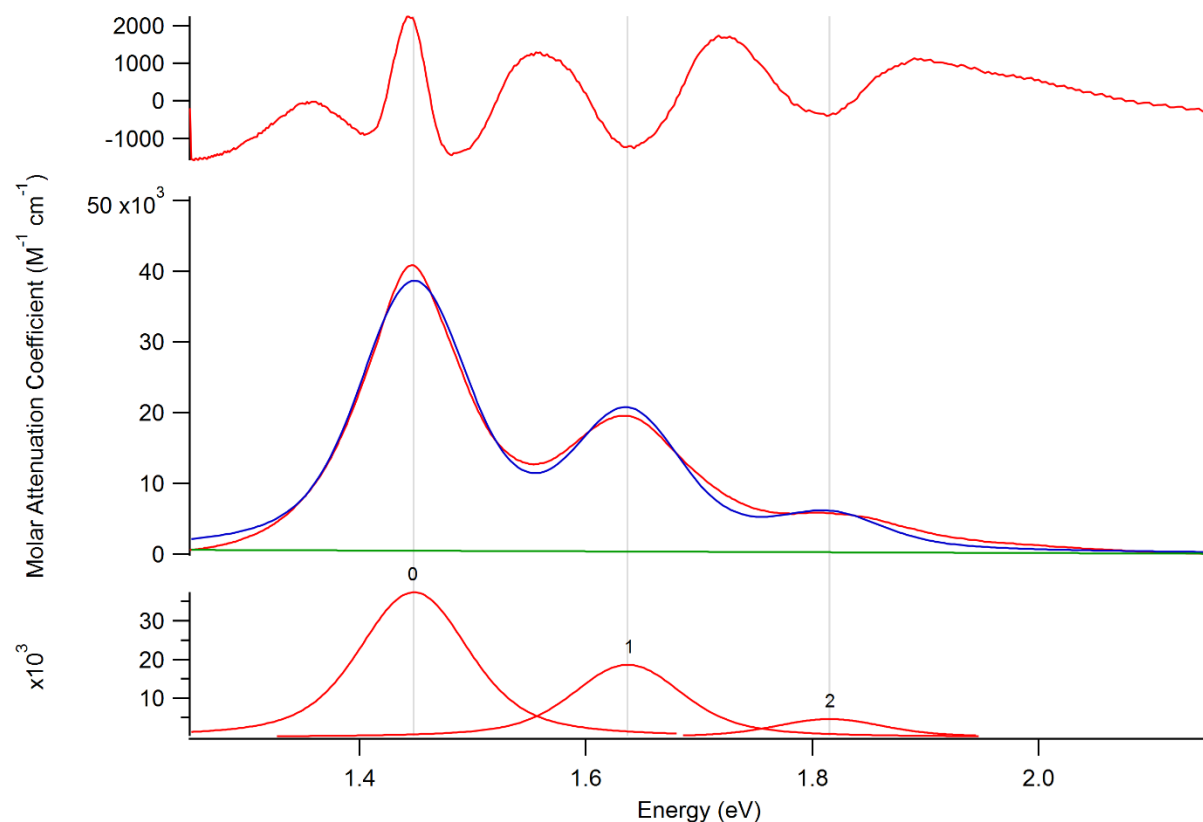


Figure S 5. Fitting results for 12 mM [Cp*₂Co][F₄TCNQ] reference solution. Top panel shows deviation of fit from spectrum. Middle panel shows sum of fit peaks (blue) and the baseline (green) over the reference spectrum (red). Bottom panel shows the three Voigt peaks used to fit the spectrum.

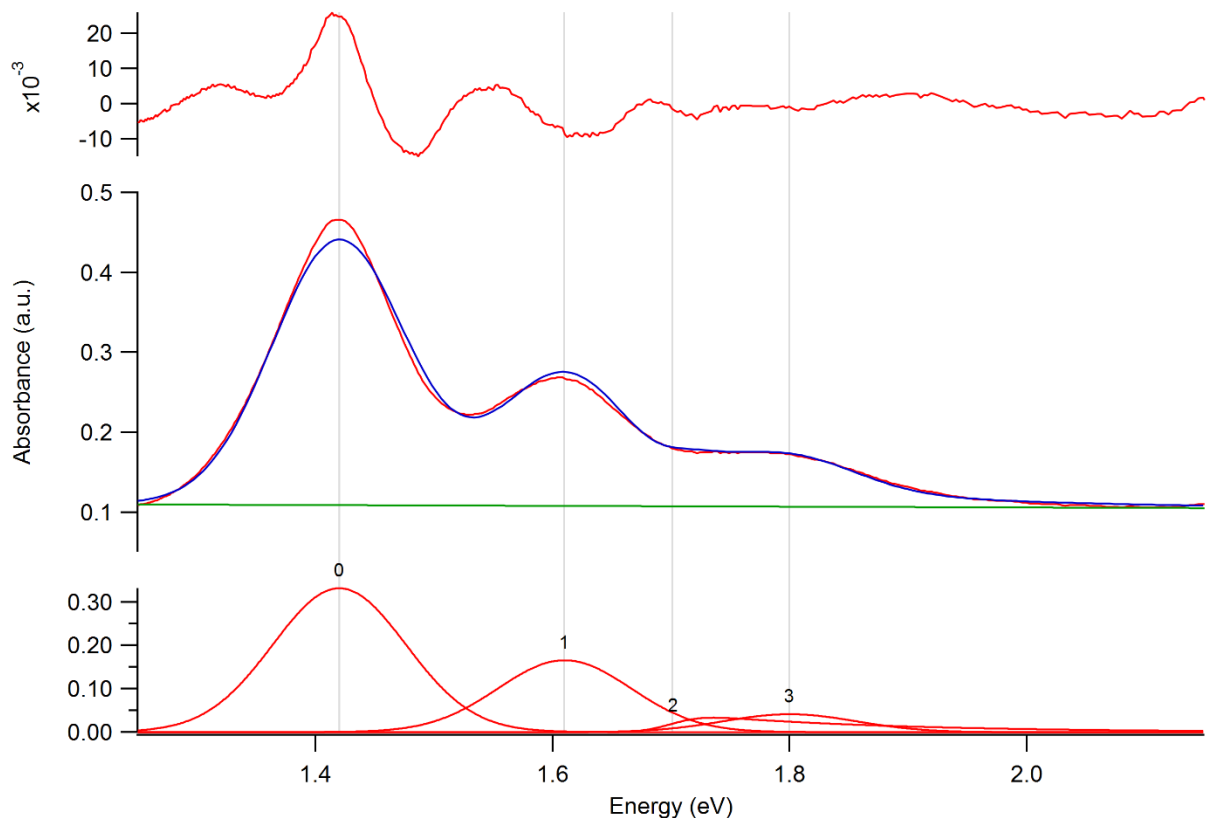


Figure S 6. Example of fitting results for a F₄TCNQ vapor-doped spiro-OMeTAD film. Top panel shows deviation of fit from the film spectrum. Middle panel shows the sum of the fit peaks (blue) and baseline (green) over the film spectrum (red). Bottom panel shows the four peaks used to fit the spectrum. Peaks 0, 1, and 3 are the Voigt (nearly Gaussian) peaks fitting the F₄TCNQ anion signal. Peak 2 is the ExpModGauss peak at 1.74 eV fitting the spiro-OMeTAD⁺ signal.

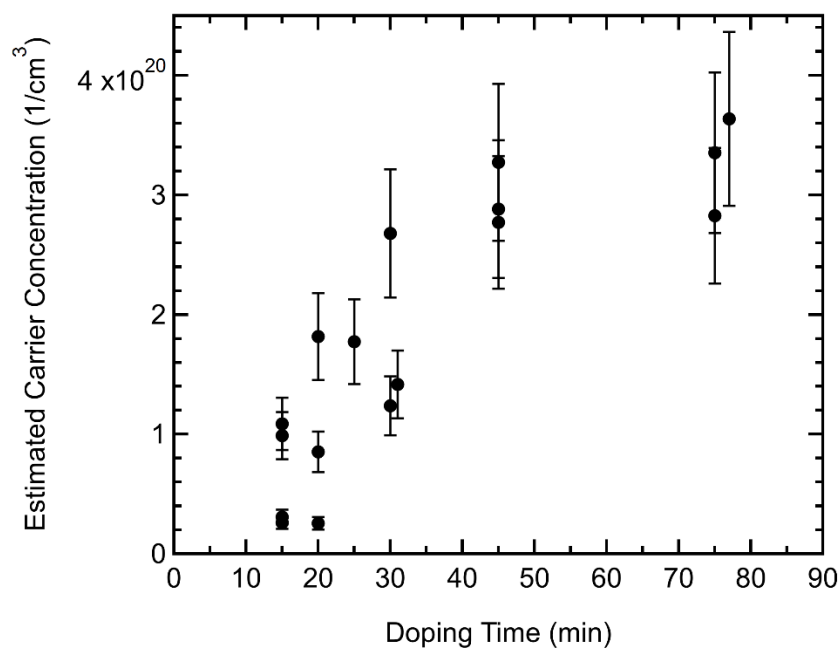


Figure S 7. Estimated carrier concentration versus doping time.

Density Estimation

Film thickness and carrier concentrations are the averages of three samples with the same doping time. Mass densities for doped films were estimated by adding the mass of F₄TCNQ molecules (from the estimated carrier concentration) to the average mass of an average undoped spiro-OMeTAD film (417 nm thick). The estimated F₄TCNQ mol% was calculated using the amount of F₄TCNQ estimated from the UV-Vis-NIR spectra and the amount of spiro-OMeTAD in a film with a density of 1.02 g/cm³.⁹

$$\frac{1.02 \text{ g}}{\text{cm}^3} \times \frac{\text{mol}}{1225.43 \text{ g}} \times N_A = 5.02 \times 10^{20} \text{ molecules/cm}^3$$

Table S 3. Average thickness and estimated mol% of spiro-OMeTAD:F₄TCNQ films depending on doping time.

Doping Time (min)	Thickness (nm)	Estimated Carrier Concentration (x 10 ²⁰ 1/cm ³)	Estimated Mass Density (g/cm ³)	Estimated mol% F ₄ TCNQ
0	417 ± 15	0	1.02 (from ref. ⁹)	0
15	495 ± 98	0.7 ± 0.4	0.92 ± 0.16	11 ± 6
20	461 ± 17	0.9 ± 0.6	0.97 ± 0.05	15 ± 9
30	479 ± 22	1.8 ± 0.6	0.97 ± 0.04	26 ± 7
45	544 ± 9	3.0 ± 0.2	0.918 ± 0.005	37 ± 2
75	506 ± 29	3.3 ± 0.3	0.99 ± 0.04	39 ± 2

Mobility

Mobility (μ) was calculated using conductivity (σ) measurements and estimated carrier concentrations (p). The hole mobility stays on the order of 10⁻⁴ cm²/V·s but some points may indicate a downward trend in mobility with increasing carrier concentration.

$$\mu = \frac{\sigma}{pq}$$

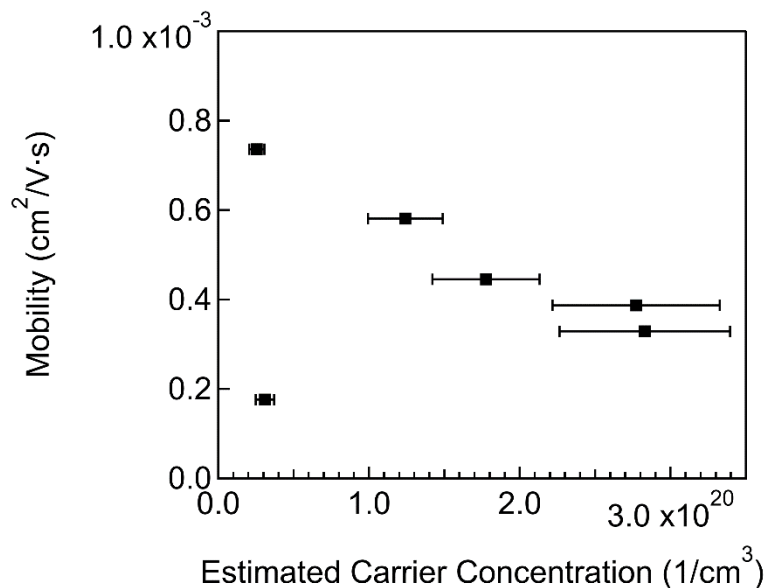


Figure S 8. Calculated hole mobility as a function of estimated carrier concentration.

Temperature-dependent Conductivity

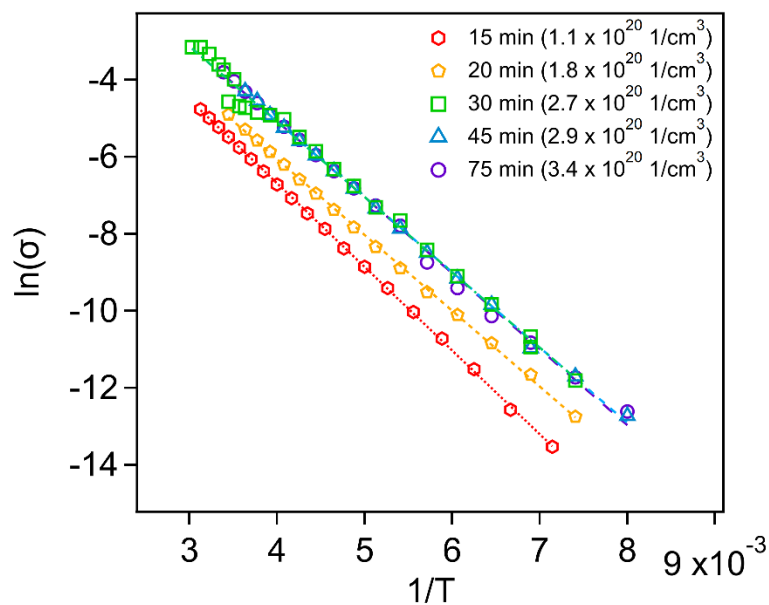


Figure S 9. Temperature-dependent conductivity plotted as the natural log of conductivity (S/cm) vs. inverse temperature (K) to show the Arrhenius relationship of thermally activated hopping.

References

- 1 J. Ilavsky, Nika: software for two-dimensional data reduction, *J. Appl. Cryst.*, 2012, **45**, 324–328.
- 2 S. D. Oosterhout, V. Savikhin, J. Zhang, Y. Zhang, M. A. Burgers, S. R. Marder, G. C. Bazan and M. F. Toney, Mixing Behavior in Small Molecule: Fullerene Organic Photovoltaics, *Chem. Mater.*, 2017, **29**, 3062–3069.

- 3 A. Vega-Flick, D. Jung, S. Yue, J. E. Bowers and B. Liao, Reduced thermal conductivity of epitaxial GaAs on Si due to symmetry-breaking biaxial strain, *Phys. Rev. Mater.*, 2019, **3**, 034603.
- 4 Gaussian 16, Revision C.01, M. J. Frisch, G. W. Trucks, H. B. Schlegel, G. E. Scuseria, M. A. Robb, J. R. Cheeseman, G. Scalmani, V. Barone, G. A. Petersson, H. Nakatsuji, X. Li, M. Caricato, A. V. Marenich, J. Bloino, B. G. Janesko, R. Gomperts, B. Mennucci, H. P. Hratchian, J. V. Ortiz, A. F. Izmaylov, J. L. Sonnenberg, D. Williams-Young, F. Ding, F. Lipparini, F. Egidi, J. Goings, B. Peng, A. Petrone, T. Henderson, D. Ranasinghe, V. G. Zakrzewski, J. Gao, N. Rega, G. Zheng, W. Liang, M. Hada, M. Ehara, K. Toyota, R. Fukuda, J. Hasegawa, M. Ishida, T. Nakajima, Y. Honda, O. Kitao, H. Nakai, T. Vreven, K. Throssell, J. A. Montgomery, Jr., J. E. Peralta, F. Ogliaro, M. J. Bearpark, J. J. Heyd, E. N. Brothers, K. N. Kudin, V. N. Staroverov, T. A. Keith, R. Kobayashi, J. Normand, K. Raghavachari, A. P. Rendell, J. C. Burant, S. S. Iyengar, J. Tomasi, M. Cossi, J. M. Millam, M. Klene, C. Adamo, R. Cammi, J. W. Ochterski, R. L. Martin, K. Morokuma, O. Farkas, J. B. Foresman, and D. J. Fox, Gaussian, Inc., Wallingford CT, 2016.
- 5 D. A. Dixon, J. C. Calabrese and J. S. Miller, Crystal and molecular structure of the 2:1 charge-transfer salt of decamethylferrocene and perfluoro-7,7,8,8-tetracyano-p-quinodimethane: $[[\text{Fe}(\text{C}_5\text{Me}_5)_2]^+ \cdot 2[\text{TCNQF}_4]^{2-}]$. The electronic structure of $[\text{TCNQF}_4]_n$ ($n = 0, 1-, 2-$), *J. Phys. Chem.*, 1989, **93**, 2284–2291.
- 6 D. T. Scholes, S. A. Hawks, P. Y. Yee, H. Wu, J. R. Lindemuth, S. H. Tolbert and B. J. Schwartz, Overcoming Film Quality Issues for Conjugated Polymers Doped with F4TCNQ by Solution Sequential Processing: Hall Effect, Structural, and Optical Measurements, *J. Phys. Chem. Lett.*, 2015, **6**, 4786–4793.
- 7 D. Kiefer, R. Kroon, A. I. Hofmann, H. Sun, X. Liu, A. Giovannitti, D. Stegerer, A. Cano, J. Hynynen, L. Yu, Y. Zhang, D. Nai, T. F. Harrelson, M. Sommer, A. J. Moulé, M. Kemerink, S. R. Marder, I. McCulloch, M. Fahlman, S. Fabiano and C. Müller, Double doping of conjugated polymers with monomer molecular dopants, *Nat. Mater.*, 2019, **18**, 149–155.
- 8 U. Bach, PhD Thesis, École Polytechnique Fédérale de Lausanne, 2000.
- 9 P. Docampo, A. Hey, S. Guldin, R. Gunning, U. Steiner and H. J. Snaith, Pore Filling of Spiro-OMeTAD in Solid-State Dye-Sensitized Solar Cells Determined Via Optical Reflectometry, *Adv. Funct. Mater.*, 2012, **22**, 5010–5019.